Chapter 10

SolarAnywhere Forecasting

Richard Perez
Atmospheric Sciences Research Center, University at Albany

Tom E. Hoff
Clean Power Research

Chapter Outline

10.1. THE SOLARANYWHERE SOLAR RESOURCE AND FORECAST DATA SERVICE

SolarAnywhere is a solar resource platform that provides seamless data access from the past to current conditions that can be forecast for every point in most of North America, Hawaii, and the Caribbean (Clean Power Research 2012).[1]

10.1.1. Historical Data

The historical portion of SolarAnywhere covers the period from 1998 to current conditions. Irradiances are derived from U.S. geostationary weather

1. Currently available in North America.

Solar Energy Forecasting and Resource Assessment. ISBN: 9780123971777

satellites using a semi-empirical model of the type described in Chapter 2. SolarAnywhere Standard Resolution includes hourly data geographically subsampled every 0.1° (~10 km) in latitude and longitude. It uses the native time and space resolution of the U.S. geostationary satellites and provides half-hourly irradiances with a ground resolution of 0.01° (~1 km). Finally, SolarAnywhere High Resolution uses cloud motion (see below) to animate satellite images between consecutive half-hourly native frames and to produce 1 min irradiances with the native satellite's 0.01° geographical resolution. (See Figure 10.1.)The new generation of U.S. geostationary satellites (GOES-R), which is expected to come online in 2015, will deliver data on a 5 min basis; this added resolution will be included in future SolarAnywhere products.

10.1.2. Forecast Data

The forecast portion of SolarAnywhere spans current conditions up to 6 d ahead. Two distinct forecasting methodologies are used as a function of the

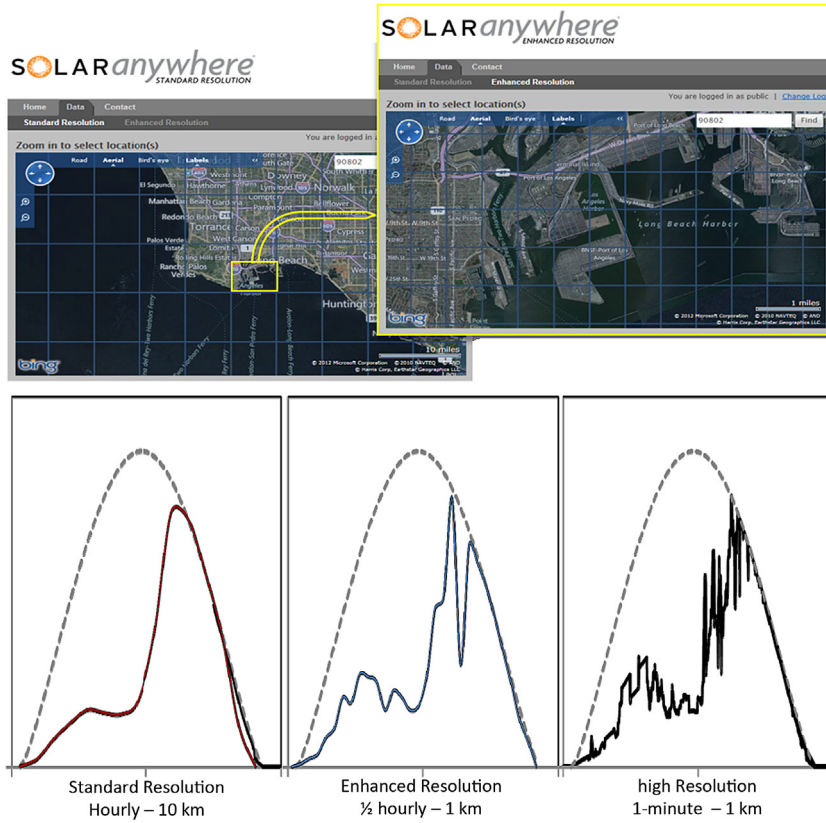

FIGURE 10.1 SolarAnywhere versions. *This figure is reproduced in color in the color section.*

considered time horizon: cloud-motion vector for short time horizons and numerical weather prediction (NWP) for long time horizons.

Short Time Horizons

The approach for short time horizons (up to a few hours ahead) consists of projecting observed solar-radiation conditions based on immediate measured solar-radiation history (i.e., a cloud-motion vector approach). The position and impact of future clouds are inferred from their motion determined from recent satellite observations. This approach is initially deterministic because the initial position of clouds affecting a solar installation is precisely known. In SolarAnywhere, the observations consist of the most recent historical satellite-derived data, as discussed previously.

Long Time Horizons

The approach for longer time horizons (hours to days) consists of NWP models. NWP models can be global (e.g., GFS 2003, ECMWF 2010) or local/regional (e.g., WRF 2010, Skamarock et al. 2005). NWP irradiance predictions are inherently probabilistic because they infer local cloud-formation probability (and indirectly transmitted radiation) through dynamic modeling of the atmosphere. NWP models cannot, at this stage of development, predict the exact position and extent of individual clouds or cloud fields affecting a given location's solar resource.

Lorenz et al. (2007) have shown that cloud-motion vector forecasts tend to provide better results than NWP forecasts up to forecast horizons of 3–4 h, beyond which NWP models perform better.

In this chapter, we present an evaluation of the short-term and long-term hourly irradiance forecast from SolarAnywhere at standard resolution. We also describe and present an initial evaluation of SolarAnywhere High Resolution forecasts delivering 1 min data up to 1 h ahead.

10.2. SOLARANYWHERE FORECAST MODELS

10.2.1. Short-Term Cloud-Motion Vector Forecasts

In standard resolution, short-term irradiance forecasts are produced using two consecutive satellite images, as discussed in Chapter 2 (see also Perez et al. 2002, 2004). Pixel-specific cloud motion is determined from these two images. The satellite images are first processed to remove solar-geometry effects. Each pixel is thus converted from sensor count to clear-sky index Kt^*.[2]

The cloud-motion vector is then determined for each individual image pixel. The methodology used in SolarAnywhere is patterned after Lorenz et al.

2. Kt^* equals the ratio between (satellite-derived) GHI and local clear-sky global irradiance GHI_{clear}.

(2007). Pixel-specific motion vectors are determined by calculating the RMSE of the difference between two consecutive image-derived *Kt** maps surrounding the considered pixel when the second grid is advected in the direction of a motion vector. The selected motion vector corresponds to the lowest RMSE. This process is repeated for each image pixel, and each pixel is assigned an individual motion vector.

*Kt** maps for subsequent hours, up to 6 h ahead,[3] are derived from localized motion. Future images are obtained by displacing the current image pixels in the direction of their motion vector. They are subsequently smoothed by averaging each pixel with its 8 surrounding intermediate-resolution neighbors representing an area of $\sim 700\ km^2$, following the pragmatic approach described by Lorenz et al. (2007).

The high-resolution (1 km) satellite images provide considerably more structural details than standard resolution (~ 10 km) satellite images. The cloud-motion vector approach can be applied to these images to generate subhourly scenes down to nearly 1 min.[4] Data streams of 1 min can be generated for (1) historical data, using motion-vector animation of two consecutive images and (2) future (forecast) data by projecting the latest image forward.

10.2.2. Numerical Weather-Prediction Forecasts

The longer-term SolarAnywhere GHI forecasts are derived from the U.S. National Digital Forecast Database (NDFD) (National Weather Service 2010). The NDFD produces gridded forecasts of sky-cover fraction for the United States. The sky-cover fraction is converted into an irradiance clear-sky index using a simple transposition model.

The NDFD sky-cover forecasts are the result of a multistep forecasting process, involving

- Global forecasts produced using NOAA's GFS model (2003). This process estimates a cloud-amount parameter (analogous to the cloud cover traditionally recorded by weather observers) from predicted relative humidity at several elevations (Xu and Randall 1996). Note that the GFS model also produces surface irradiances. These irradiances, however, are not distributed in the gridded products disseminated as part of the NDFD—hence SolarAnywhere's reliance on cloud amount.

3. The current version of SolarAnywhere uses only the satellite's visible channel to determine cloud indices; hence, cloud motion can be determined only after sunup. As a result, *N*-h forecasts are only available $N + 1$ h after sunrise. The new version of SolarAnywhere uses the infrared satellite channels in addition to the visible channel, thus making it possible to infer nighttime cloud motion and so overcome this limitation.

4. The achievable time resolution is defined by the ratio of cloud speed to the image's spatial resolution (1 km), which defines the size of the cloud structures that can be captured to determine variability at a given time scale.

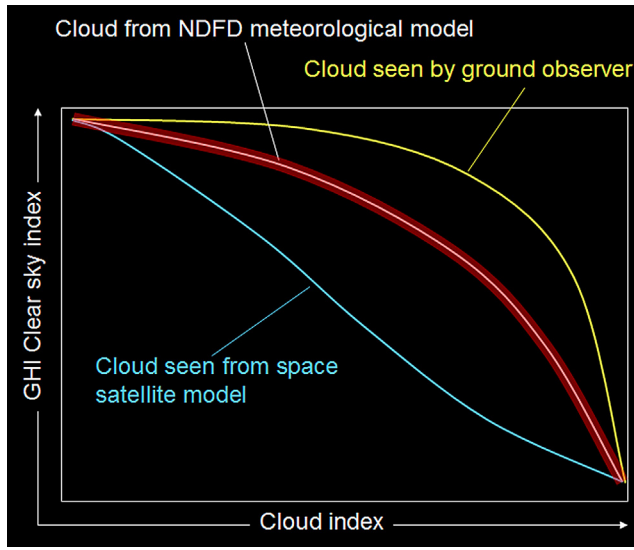

FIGURE 10.2 Functions for converting cloud cover, index, or amount to the GHI clear-sky index (Kt^*). These functions are dependent on the nature of the cloud index: whether observed or measured cloud cover at the ground (*yellow line*) or seen from space (*blue line*) or the cloud amount probabilistically generated by an NWP model (*red line*). *This figure is reproduced in color in the color section.*

- Modification of the GFS forecast by regional NOAA offices using a variety of tools, including regional/local models and human input; this process often results in enhancing cloudiness.
- Reassembling of the regional NOAA offices' modified forecasts into a national grid with a nominal geographical resolution of ~5 km in the continental United States.

They are produced on a 3 h basis for up to 3 d ahead and on a 6 h basis 3–6 d ahead.

The 5 km NDFD grid is subsampled down to the SolarAnywhere Standard Resolution grid size of $0.1^\circ \times 0.1^\circ$ latitude and longitude, and converted into irradiances by taking the closest NDFD grid point.

Hourly cloud amounts are first produced from the NDFD 3 h or 6 h data via linear time interpolation. Global irradiances are then produced using a multisite empirical fit between the cloud amount and the GHI clear-sky index (see Perez et al. 2007).

This conversion of cloud amount to irradiance is similar to the earlier cloud-cover–irradiance models developed at a time when human-observed cloud cover was one of the few proxies available to estimate the solar resource (e.g., the relationship of Kasten and Czeplak 1979). It is also similar to the cloud index–clear-sky index models used in satellite models (e.g., see Chapter 2). There are intrinsic differences, however, in quantifying cloud cover between human observation, cloud index in satellite remote sensing, and cloud amount

in NWP modeling. The differences in the cloud–irradiance relationships are seen in Figure 10.2. The cloud cover represents clouds seen by an observer at the ground, reporting the percentage of the sky obstructed from his/her vantage point. The cloud index represents clouds seen from the top and quantified using a satellite's onboard-sensor count. The cloud amount represents a probabilistic cloud percentage produced by NWP models.

10.3. MODEL EVALUATION: STANDARD RESOLUTION

All the NDFD forecasts tested in the present evaluation originate once daily at 11:00 GMT[5]—that is, the time before sunrise in the continental United States (CONUS) and include same-day and next-day forecasts, and day-ahead (2, 3, 4, 5, 6 d) forecasts.

All cloud-motion and NWP forecasts are validated against single-point ground-truth stations. In addition, the ability of forecast models to account for local microclimatology is investigated by observing the distribution of mean predictions over extended areas.

10.3.1. Single-Point Ground-Truth Validation

Hourly forecasts are tested against irradiance data from each station of the Surface Radiation (SURFRAD) network (National Weather Service 2010), including Desert Rock, Nevada; Fort Peck, Montana; Boulder, Colorado; Sioux Falls, South Dakota; Bondville, Illinois; Goodwin Creek, Mississippi; and Penn State, Pennsylvania.

These stations cover several distinct climatic environments ranging from arid (Desert Rock) to humid continental (Penn State) and some subtropical influence (Goodwin Creek) to the northern Great Plains (Fort Peck). Boulder is a challenging site for all types of solar-radiation models because of its high elevation ($\sim$2000 m) and its position at the Rocky Mountains' eastern edge at the junction between two weather regimes.

The validation period spans a little over one year, from August 23, 2008, to August 31, 2009 (Perez et al. 2010b).

Validation Metrics

We first consider the well-known and commonly accepted mean bias and root mean square errors (respectively MBE and RMSE) resulting from the direct comparison of hourly forecasts and hourly measurements. The MBE quantifies the overall bias of the considered model while the RMSE is a measure of its dispersion.[6]

5. Therefore, the results here represent a worse-case evaluation of the SolarAnywhere forecasts because, operationally, forecasts are refreshed every hour.

6. Note that another measure of dispersion, mean absolute error, was recently recommended as the preferred methodology to report relative (percentage) errors (Hoff et al. 2012).

We also consider two metrics that quantify the ability of a model to reproduce observed frequency distributions. The first metric is the Kolmogorov-Smirnoff integral (KSI) goodness-of-fit test (Espinar et al. 2008) recommended by the International Energy Agency Solar Heating & Cooling Programme, Task 36 for data benchmarking (IEA-SHCP 2010).

The KSI metric (equation 10.1) is obtained by integrating the absolute difference between the modeled and measured cumulative frequency distributions of the considered variable (in this case irradiance), normalized to the KSI critical value *Vc*. *Vc* is a goodness-of-fit coefficient that specifies how close the experimental (modeled) cumulative distribution should be to the reference (measured) distribution based on the number of available data samples. The Kolmogorov-Smirnoff approach assumes that the higher the number of experimental data samples, the closer the modeled distribution to the actual distribution—hence the smaller the critical value. We retain here the National Institute of Standards and Technology (NIST approximation of $Vc = 1.63/\sqrt{n}$ (NIST 2010, IEA-SHCP 2010), where n is the number of considered data samples.

$$KSI = \frac{\int_0^{I_{\max}^{ref}} \left|\varphi\left(I^{\text{modeled}}\right) - \varphi\left(I^{\text{measured}}\right)\right| dI}{Vc} \tag{10.1}$$

The expression $\varphi(I^{\text{modeled}})$ is the cumulative frequency distribution of the modeled (forecast) irradiance and $\varphi(I^{\text{measured}})$ is the cumulative frequency distribution of the measured reference irradiance. A KSI score of the order of, or better than,100% is generally considered acceptable. An interpretation of this is that the mean absolute difference between the measured and modeled distributions is equal to or smaller than the critical difference. (The example in Figure 10.3 illustrates a score slightly higher than 100%—i.e., the KSI area shown in the bottom half of the figure is slightly larger than the area below the critical dotted line.)

The second metric, termed OVER (equation 10.2), is calculated by integrating the absolute difference between the modeled distribution and the measured distribution plus or minus a buffer determined by the number of consider data points.

$$\text{OVER} = \frac{\int_0^{I_{\max}^{ref}} \left(\text{MAX}\left(0, \left|\varphi\left(I^{\text{modeled}}\right) - \varphi\left(I^{\text{measured}}\right)\right| - Vc\right) dI}{Vc} \tag{10.2}$$

An OVER score of 0% indicates that the model always lies between the two critical dotted lines. (In Figure 10.3, the score is roughly equal to 30%—the modeled distribution is partly outside the critical envelope and the resulting OVER shaded area represents 30% of the critical area that would be obtained by integrating the difference between the critical (dotted) line and the actual distribution.

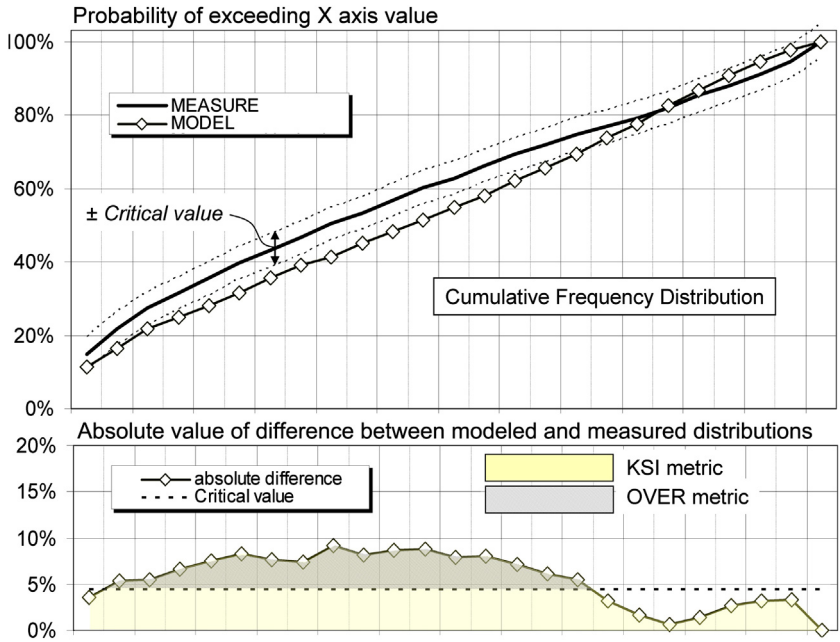

FIGURE 10.3 KSI and OVER metrics. *Top:* modeled and measured cumulative probability distributions and the critical value envelope around the measured distribution. *Bottom:* absolute difference between the two distributions. The metrics are obtained by integrating the area under the curves: KSI (*lightly shaded*); OVER (*striped*). *This figure is reproduced in color in the color section.*

The performance of the forecast models is evaluated in reference to a simple persistence model that consists of projecting an exact measure of (hourly) irradiance at forecast initiation into the future, assuming that conditions of the clearness of the sky (Kt^*) remain unchanged and only the precisely predictable solar-geometry effects change. Same-day persistence is obtained by time extrapolation of measured hourly irradiance using a constant clear-sky index. Next-day (and multiday) persistence is obtained by calculating the current day's mean daily measured clear-sky index as the ratio of the measured daily irradiance to the clear-sky daily irradiance and then applying this clear-sky index to all hours in the following days.

Results

All forecasts are validated against the same set of experimental values. Therefore, because 6 h cloud-motion forecasts cannot be generated until the sun is up,[7] the experimental "common validation denominator pool" is limited to points 6 h or more after sunrise.

7. This is because the satellite model used in this evaluation uses only the satellite's visible channel. The next version of SolarAnywhere, which uses the satellite's IR channels, will not have this limitation.

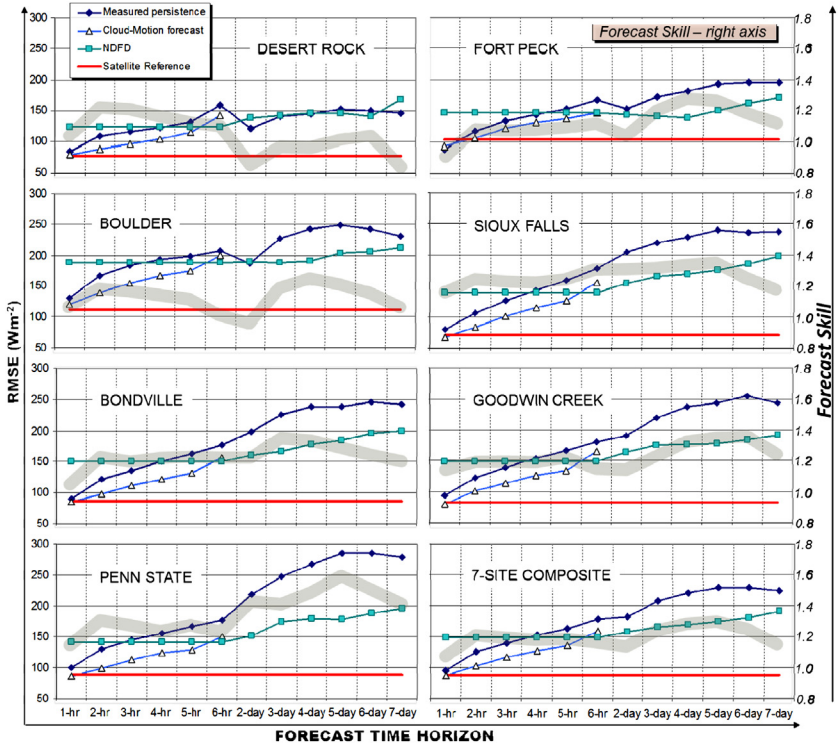

FIGURE 10.4 Annual RMSE and forecast skill as a function of forecast time horizon. *This figure is reproduced in color in the color section.*

Figure 10.4 plots both the yearly RMSE and the forecasting-skill trends for all sites and all models as a function of the forecast time horizon. The RMSE is plotted against the left axis and the forecasting skill, which is defined here as the ratio of persistence RMSE to forecast-model RMSE, is plotted against the right axis. Also shown is the performance of the SUNY semi-empirical satellite-to-irradiance model (Perez et al. 2002, 2004) for the same sites so as to provide an external model-performance reference. The reference satellite model's RMSE appears as a horizontal line across all forecasts horizons.

Figure 10.5 provides a qualitative appreciation of performance with a sample of measured versus modeled scatter plots at four of the seven sites, including Bondville, Boulder, Desert Rock, and Goodwin Creek, using an hourly time interval. This illustrative sample includes the reference satellite model, the 1 and 3 h cloud-motion forecasts, the next-day and 3 d NDFD forecasts, and the same time horizons (1 h, 3 h, 1 d, and 3 d ahead) for the persistence-model benchmark.

Tables 10.1 and 10.2 provide a detailed view of the results summarized in Figure 10.4. They report, respectively, the absolute MBE and RMSE

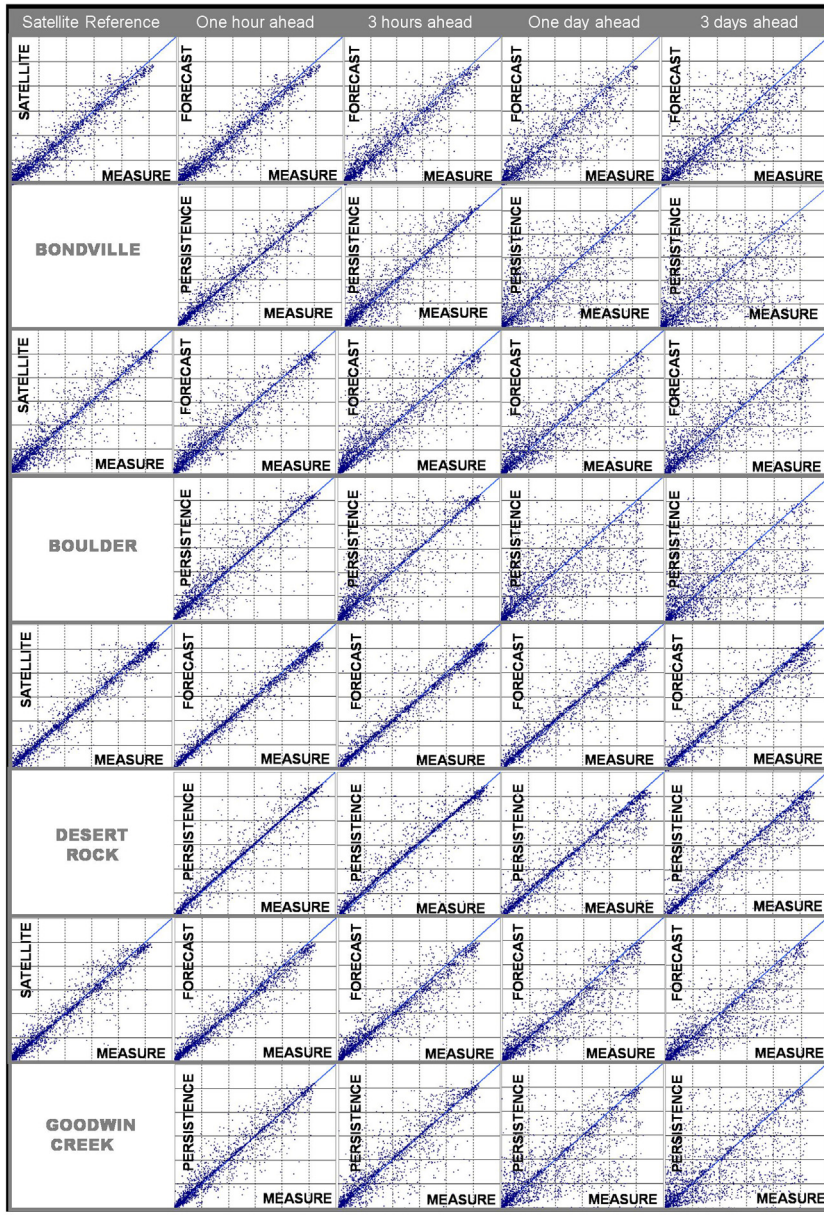

FIGURE 10.5 Comparison of hourly forecasts and persistence versus measured GHI scatter plots for 1, 3 h ahead and 1, 3 d ahead. Scatter plots provide a qualitative, visual appreciation of model performance showing that the core of forecast points are closer to the 1:1 line and exhibit fewer outlying points. *This figure is reproduced in color in the color section.*

TABLE 10.1 Yearly and seasonal MBE-Metric Summary (Wm^{-2})

	MBE	Desert Rock		Fort Peck		Boulder		Sioux Falls		Bondville		Godwin Creek		Penn State	
ALL YEAR	Mean observed GHI	498		357		369		364		349		397		323	
	Clearness index[a]	90%		75%		71%		76%		69%		76%		66%	
	Satellite model error	1		−4		7		14		−3		−1		4	
	Forecast/persistence	Fcst	Prst	Fcst	Prst	Fcst	Prst	Fcst	Prst	Fcst	Prst	Fcst	Prst	Fcst	Prst
	1 h ahead	1	11	−3	8	13	20	15	7	−2	6	−5	6	−4	5
	2 h ahead	2	18	0	12	26	36	13	11	−3	11	−8	7	−7	6
	3 h ahead	5	20	−3	13	33	47	9	10	−3	15	−13	4	−7	5
	4 h ahead	5	16	−5	10	36	50	3	4	−2	17	−20	−3	−4	−3
	5 h ahead	1	3	−7	2	38	44	0	−7	−3	12	−19	−14	−2	−16
	6 h ahead	−13	−23	−6	−13	38	28	−7	−19	0	3	−28	−31	−2	−32
	1 d (same day)	−5		13		−22		−12		−14		−33		−28	
	2 d (next day)	−10	0	12	−2	−25	1	−17	−2	−19	−3	−35	−3	−30	−1
	3 d	−16	0	14	−2	−23	0	−18	−3	−15	−1	−46	−4	−40	−2
	4 d	−12	−1	17	−2	−14	2	−14	−2	−14	−1	−48	−4	−35	−2
	5 d	−7	−1	22	−3	−7	0	−8	−1	−13	−1	−51	−4	−36	−3
	6 d	1	−1	24	−4	−6	−2	−13	−2	−14	−1	−48	−4	−40	−3
	7 d	−30	−2	11	−4	−11	−2	−17	−2	−17	2	−43	−5	−48	−4

(*Continued*)

TABLE 10.1 Yearly and seasonal MBE-Metric Summary (Wm^{-2})—cont'd

	MBE	Desert Rock		Fort Peck		Boulder		Sioux Falls		Bondville		Godwin Creek		Penn State	
WINTER	Mean observed GHI	236		159		215		160		137		189		140	
	Clearness index[a]	82%		51%		78%		77%		73%		72%		73%	
	Satellite model error	12		−49		18		23		32		17		47	
	1 h ahead	11	14	−63	10	14	11	9	8	17	5	7	10	27	6
	2 h ahead	10	23	−66	15	7	20	0	14	9	9	6	11	16	10
	3 h ahead	11	28	−70	17	−1	24	−9	17	0	11	3	5	12	13
	4 h ahead	13	26	−72	13	−7	23	−15	15	2	13	2	0	12	12
	5 h ahead	12	17	−69	5	−11	12	−17	8	4	11	3	−7	21	5
	6 h ahead	7	0	−60	−5	−23	−2	−25	−1	25	2	11	−25	18	−9
	1 d (same day)	−13		−47		−37		−39		−15		−9		−44	
	2 d (next day)	−15	6	−34	3	−31	5	−41	5	−21	3	−13	6	−37	3
	3 d	−20	5	−26	1	−38	8	−33	8	−7	11	−23	7	−33	6
	4 d	−28	3	−22	3	−34	8	−24	12	−7	11	−26	5	−27	9
	5 d	−30	2	−19	4	−34	10	−8	11	6	14	−25	10	−30	6
	6 d	−30	1	−22	7	−36	8	−1	9	9	6	−16	11	−30	3
	7 d	−31	2	−24	9	−40	6	0	8	17	8	−14	15	−37	3

SPRING	Mean observed GHI	548		377		416		391		373		416		361	
	Clearness index[a]	90%		72%		68%		73%		65%		72%		64%	
	Satellite model error	7		−3		−1		11		−2		1		3	
	1 h ahead	5	14	2	13	12	21	18	7	8	7	−4	4	0	8
	2 h ahead	7	22	7	21	20	35	18	11	5	12	−13	4	1	9
	3 h ahead	12	26	4	24	20	42	15	11	9	16	−24	−6	1	5
	4 h ahead	11	25	0	23	18	41	6	6	6	15	−37	−19	1	−7
	5 h ahead	5	13	−6	17	17	31	3	−5	5	9	−37	−34	1	−25
	6 h ahead	−6	−11	4	4	4	8	2	−16	16	−2	−37	−51	7	−46
	1 d (same day)	−6		10		−35		−18		−17		−63		−20	
	2 d (next day)	−15	1	0	−2	−40	5	−26	−3	−23	−12	−46	−5	−35	−4
	3 d	−28	4	−2	−4	−46	5	−38	−8	−23	−10	−50	−10	−42	−6
	4 d	−21	8	1	−5	−33	6	−35	−8	−28	−10	−68	−13	−44	−3
	5 d	−18	9	3	−7	−13	5	−30	−7	−25	−3	−56	−14	−42	0
	6 d	−9	10	9	−8	−12	10	−35	−6	−34	2	−51	−12	−47	6
	7 d	−41	8	4	−9	−20	12	−29	−1	−49	8	−57	−8	−62	12
SUMMER	Mean observed GHI	617		454		432		451		443		510		403	
	Clearness index[a]	90%		80%		70%		79%		70%		81%		66%	
	Satellite model error	−7		−3		4		12		−19		−8		−15	
	1 h ahead	−6	9	2	3	11	21	13	7	−19	5	−8	3	−20	3

(*Continued*)

TABLE 10.1 Yearly and seasonal MBE-Metric Summary (Wm^{-2})—cont'd

	MBE	Desert Rock		Fort Peck		Boulder		Sioux Falls		Bondville		Godwin Creek		Penn State	
	2 h ahead	−3	15	7	4	34	40	12	7	−15	11	−9	4	−23	4
	3 h ahead	−1	13	4	4	55	58	9	3	−14	16	−12	4	−21	3
	4 h ahead	−2	5	4	−2	67	66	6	−5	−10	19	−18	1	−13	−6
	5 h ahead	−9	−13	3	−12	76	64	3	−19	−13	14	−19	−10	−12	−20
	6 h ahead	−28	−49	−2	−28	68	52	−8	−30	−16	6	−41	−24	−10	−30
	1 d (same day)	−15		18		−42		−13		−24		−21		−45	
	2 d (next day)	−22	0	23	−4	−53	2	−15	−1	−27	−4	−36	−8	−40	0
	3 d	−24	0	29	−7	−41	4	−7	−2	−23	−5	−60	−10	−68	−1
	4 d	−19	0	31	−7	−31	9	−3	1	−21	−5	−51	−14	−52	0
	5 d	−8	0	39	−8	−30	8	0	3	−28	−4	−68	−14	−55	2
	6 d	7	0	38	−9	−35	3	−23	4	−29	0	−72	−12	−63	4
	7 d	−46	1	10	−6	−40	2	−49	5	−35	5	−60	−12	−61	2
FALL	Mean observed GHI	406		246		291		250		265		327		253	
	Clearness index[a]	90%		76%		72%		72%		70%		76%		69%	
	Satellite model error	0		24		15		18		6		1		11	
	1 h ahead	2	11	17	10	20	20	17	9	3	8	−7	11	1	4

2 h ahead	2	16	14	13	29	34	16	15	4	15	−9	13	−3	6
3 h ahead	3	19	10	13	32	41	11	19	6	22	−14	14	−5	5
4 h ahead	5	19	6	7	30	42	7	17	8	26	−15	10	−2	1
5 h ahead	4	7	2	−1	26	37	4	10	9	21	−13	−2	−1	−12
6 h ahead	−14	−16	−7	−18	8	22	−7	−7	0	13	−24	−19	−7	−30
1 d (same day)	20		33		41		13		10		−17		6	
2 d (next day)	21	0	30	−6	37	3	6	2	10	−3	−18	−6	7	3
3 d	18	1	26	−7	38	4	2	2	14	−6	−21	−10	6	6
4 d	22	1	31	−5	46	6	0	6	21	−5	−22	−13	13	9
5 d	24	2	31	−5	51	9	15	9	27	−5	−26	−14	12	9
6 d	21	4	35	−1	63	10	30	10	33	−3	−25	−13	17	12
7 d	11	5	36	−3	59	5	62	13	45	0	−23	−13	3	15

[a]*GHI/GHI clear*

TABLE 10.2 Yearly and Seasonal RMSE-Metric Summary (Wm^{-2})

	RMSE	Desert Rock		Fort Peck		Boulder		Sioux Falls		Bondville		Godwin Creek		Penn State	
ALL YEAR	Mean observed GHI	498		357		369		364		349		397		323	
	Clearness index*	90%		75%		71%		76%		69%		76%		66%	
	Satellite model error	77		103		112		72		87		83		89	
	Forecast/persistence	Fcst	Prst	Fcst	Prst	Fcst	Prst	Fcst	Prst	Fcst	Prst	Fcst	Prst	Fcst	Prst
	1 h ahead	80	85	94	88	120	130	68	80	85	91	80	93	86	100
	2 h ahead	88	109	106	118	139	167	84	106	98	122	101	123	99	131
	3 h ahead	96	118	123	135	154	183	102	127	112	135	114	139	113	145
	4 h ahead	104	123	132	145	166	193	115	142	122	150	127	154	124	155
	5 h ahead	116	133	138	154	175	199	126	159	132	164	134	166	129	166
	6 h ahead	142	160	147	168	200	207	155	178	156	177	166	181	150	176
	1 d (same day)	125		148		188		140		151		149		141	
	2 d (next day)	139	122	145	154	189	187	155	205	161	199	164	191	152	218
	3 d	142	141	142	174	188	227	165	220	167	226	176	219	174	247
	4 d	147	145	140	181	191	242	170	229	178	238	177	237	179	267
	5 d	147	152	151	194	203	249	176	240	184	239	178	243	179	285
	6 d	141	150	162	196	206	242	186	235	196	246	185	254	188	284
	7 d	169	147	172	196	212	231	198	238	200	243	193	243	196	278

WINTER	Mean observed GHI	236		159		215		160		137		189		140	
	Clearness index*	82%		51%		78%		77%		73%		72%		73%	
	Satellite model error	53		126		74		52		76		53		76	
	1 h ahead	46	53	107	26	64	53	48	36	60	52	48	53	57	42
	2 h ahead	48	65	105	37	71	71	58	54	66	61	59	67	57	59
	3 h ahead	59	78	109	44	81	82	69	68	74	73	66	80	59	64
	4 h ahead	70	84	112	50	85	87	78	80	81	81	70	87	65	67
	5 h ahead	74	88	115	58	89	93	76	83	79	82	80	92	71	66
	6 h ahead	85	94	117	67	108	98	96	83	102	83	110	101	90	68
	1 d (same day)	102		122		130		112		91		84		94	
	2 d (next day)	114	137	98	117	117	144	100	133	105	132	99	133	94	109
	3 d	107	153	93	99	125	141	111	125	88	136	121	147	111	143
	4 d	125	163	81	108	127	149	105	148	121	164	121	162	103	148
	5 d	126	170	85	105	137	170	102	138	84	150	128	157	112	145
	6 d	128	167	94	117	136	154	101	135	97	149	119	163	101	141
	7 d	133	151	100	99	143	151	108	130	106	127	126	175	112	130
SPRING	Mean observed GHI	548		377		416		391		373		416		361	
	Clear Sky Index	90%		72%		68%		73%		65%		72%		64%	
	Satellite model error	68		117		129		74		93		86		85	
	1 h ahead	86	97	110	88	125	126	69	84	93	101	92	115	83	99

(*Continued*)

TABLE 10.2 Yearly and Seasonal RMSE-Metric Summary (Wm^{-2})—cont'd

	RMSE	Desert Rock		Fort Peck		Boulder		Sioux Falls		Bondville		Godwin Creek		Penn State	
	2 h ahead	95	139	124	119	141	165	90	112	109	136	122	152	99	136
	3 h ahead	111	143	141	135	157	175	107	135	123	145	144	178	118	154
	4 h ahead	115	142	148	146	170	186	126	150	137	159	164	199	137	168
	5 h ahead	127	147	155	157	180	199	133	166	151	175	174	209	143	182
	6 h ahead	152	166	160	172	219	217	171	180	181	188	198	226	162	194
	1 d (same day)	139		154		195		136		164		186		143	
	2 d (next day)	154	134	161	159	199	222	153	236	168	239	203	231	156	263
	3 d	159	154	150	190	196	275	184	253	176	276	203	269	173	292
	4 d	163	154	147	199	209	277	189	262	172	298	207	274	184	308
	5 d	166	165	153	206	231	284	194	281	193	288	203	284	182	328
	6 d	160	171	170	223	245	273	207	277	219	293	217	301	191	322
	7 d	180	177	177	225	251	259	214	294	228	306	228	276	205	326
SUMMER	Mean observed GHI	617		454		432		451		443		510		403	
	Clearness index*	90%		80%		70%		79%		70%		81%		66%	
	Satellite model error	99		99		124		80		100		97		113	
	1 h ahead	99	100	91	111	143	170	80	97	100	108	92	103	112	131
	2 h ahead	110	119	109	149	175	214	98	127	115	145	113	135	127	164

	3 h ahead	111	132	129	169	189	233	120	150	129	160	120	145	142	181
	4 h ahead	124	144	142	180	204	245	129	167	138	178	129	157	152	191
	5 h ahead	138	157	150	188	212	246	148	190	150	197	131	175	155	204
	6 h ahead	169	199	160	204	224	252	176	217	167	217	170	190	183	213
	1 d (same day)	146		167		221		171		178		146		176	
	2 d (next day)	165	133	159	173	228	197	192	229	193	216	171	204	186	234
	3 d	170	154	165	196	225	241	184	243	204	227	194	225	222	268
	4 d	172	155	164	207	217	277	194	249	222	221	193	259	225	299
	5 d	170	169	181	220	221	290	201	264	226	227	196	241	223	319
	6 d	154	164	189	213	221	284	212	258	231	264	198	247	237	325
	7 d	204	174	202	212	229	280	233	254	228	254	207	240	237	322
FALL	Mean observed GHI Clearness index* Satellite model error	406 90% 62		246 76% 70		291 72% 80		250 72% 63		265 70% 59		327 76% 65		253 69% 60	
	1 h ahead	55	56	59	62	85	84	49	52	58	63	55	58	60	70
	2 h ahead	62	67	67	76	97	112	54	69	68	89	66	81	71	92
	3 h ahead	69	74	83	93	110	131	64	86	84	107	81	93	76	96
	4 h ahead	72	78	88	103	120	142	80	100	89	116	94	109	83	109
	5 h ahead	83	91	92	115	129	148	90	114	97	115	102	119	91	118

(*Continued*)

TABLE 10.2 Yearly and Seasonal RMSE-Metric Summary (Wm^{-2})—cont'd

RMSE	Desert Rock		Fort Peck		Boulder		Sioux Falls		Bondville		Godwin Creek		Penn State	
6 h ahead	113	111	114	130	159	150	110	134	128	116	144	132	102	132
1 d (same day)	81		100		141		86		96		116		99	
2 d (next day)	77	69	102	127	135	146	91	133	108	158	106	144	109	178
3 d	83	84	95	142	136	181	121	160	112	209	117	179	119	182
4 d	88	87	93	152	149	179	115	171	124	209	121	195	125	174
5 d	85	87	102	151	158	183	126	175	133	194	126	195	125	194
6 d	92	82	111	147	155	195	129	151	143	197	147	202	123	205
7 d	103	79	116	156	156	164	134	159	141	203	152	205	138	196

observed at all sites for all time horizons over the 1 yr period for the forecast models and persistence benchmarks. Results are reported yearly as well as seasonally. Forecasts from 1 to 6 h are cloud-motion forecasts, and same-day to 6 d-ahead forecasts are NDFD forecasts. All NWP forecasts analyzed here for same-day and multiday predictions have an origination time of 11:00 GMT.

Tables 10.3 and 10.4 report the annual KSI and OVER statistics for all sites, forecast time horizons, satellite references, and persistence benchmarks. It is helpful to refer to Figure 10.3 to appreciate the percentage scores presented in the tables. In Table 10.3, a score of 100% extracted from equation 10.1 would represent a mean difference between the model and reference distributions equal to the difference between the KSI critical (dotted) line and the reference distribution. As stated above, a KSI score below 100% indicates that the model distribution is closer on average than the critical line, while a score over 100% indicates that the model exceeds the critical departure on average. In Table 10.4, the scores extracted from equation 10.2 report the cumulative departure of the model distribution beyond the critical dotted lines above or below the reference distribution. As indicated previously, an OVER score of 0% indicates that the model distribution always lies between the test distribution and the upper or lower critical lines; the higher the score, the worse the model performance.

Discussion

The most important observation to make based on these results is that cloud-motion forecasts are almost always better than persistence forecasts derived from actual onsite measurements, even after a forecast time horizon as short as 1 h. In addition, it is interesting to note that the RMSE indicates that the 1 h forecasts actually have a lower RMSE than the satellite model at all sites but Boulder: Despite the loss of deterministic information due to cloud motion, the image smoothing inherent to the forecasts—via convergence and divergence of motion vectors, and additional postprocessing pixel averaging—results in decreasing short-term dispersion. Hence, lowering the resolution of the satellite model via image smoothing in effect appears to increase short-term accuracy as quantified by the RMSE-dispersion metric. The probable reason for this observation is small satellite-navigation errors, combined with image subsampling in the SolarAnywhere Standard Resolution model, which sometimes results in large errors when, for instance, a cloud is selected by subsampling over the test location where a cloud is not present. Note that this improvement technique for pixel-averaging performance is known and was discussed by, for example, Stuhlmann et al. (1990) when developing their physical satellite–irradiance model. This does not apply when images are not subsampled: A recent analysis by Hoff and Perez (2013) shows that properly navigated imaging using native satellite resolution in the enhanced-resolution SolarAnywhere delivers higher model accuracy.

TABLE 10.3 Annual KSI-Metric Summary

KSI	Desert Rock		Fort Peck		Boulder		Sioux Falls		Bondville		Godwin Creek		Penn State		All Sites	
Satellite model error	23%		19%		21%		30%		55%		43%		40%		33%	
Forecast/persistence	Fcst	Prst	Fcst	Prst	Fcst	Prst	Fcst	Prst	Fcst	Prst	Fcst	Prst	Fcst	Prst	Fcst	Prst
1 h ahead	39%	19%	13%	18%	62%	45%	32%	15%	56%	13%	56%	16%	56%	10%	45%	20%
2 h ahead	37%	33%	20%	26%	84%	86%	32%	23%	58%	16%	66%	21%	60%	11%	51%	31%
3 h ahead	39%	43%	15%	29%	102%	112%	45%	23%	58%	30%	82%	28%	62%	13%	58%	40%
4 h ahead	47%	51%	18%	20%	109%	125%	63%	32%	57%	36%	97%	33%	66%	29%	65%	47%
5 h ahead	55%	60%	22%	22%	121%	118%	81%	48%	71%	24%	103%	58%	77%	55%	76%	55%
6 h ahead	71%	94%	28%	47%	117%	102%	90%	65%	81%	22%	138%	97%	83%	89%	87%	74%
	64%		61%		89%		43%		59%		108%		70%			
2 d (next day)	65%	64%	63%	55%	117%	104%	66%	49%	74%	67%	113%	117%	75%	72%	82%	76%
3 d	69%	66%	65%	55%	123%	105%	70%	52%	75%	65%	139%	121%	99%	77%	92%	77%
4 d	62%	65%	76%	58%	140%	106%	70%	51%	82%	64%	144%	122%	89%	82%	95%	78%
5 d	61%	63%	87%	55%	145%	106%	86%	49%	93%	64%	156%	122%	97%	83%	104%	77%
6 d	63%	63%	99%	54%	159%	107%	121%	53%	106%	58%	151%	121%	115%	82%	116%	77%
7 d	67%	62%	104%	53%	161%	108%	137%	51%	121%	56%	146%	122%	134%	82%	124%	76%

TABLE 10.4 Annual Over-Metric Summary

OVER	Desert Rock		Fort Peck		Boulder		Sioux Falls		Bondville		Godwin Creek		Penn State		All Sites	
Satellite model error	0%		0%		0%		0%		6%		0%		3%		1%	
Forecast/persistence	Fcst	Prst	Fcst	Prst	Fcst	Prst	Fcst	Prst	Fcst	Prst	Fcst	Prst	Fcst	Prst	Fcst	Prst
1 h ahead	15%	0%	0%	0%	30%	0%	0%	0%	5%	0%	5%	0%	1%	0%	8%	0%
2 h ahead	10%	0%	0%	0%	60%	58%	10%	0%	10%	0%	10%	0%	0%	0%	14%	8%
3 h ahead	6%	0%	0%	0%	84%	102%	15%	0%	5%	0%	50%	0%	0%	0%	23%	15%
4 h ahead	15%	6%	0%	0%	95%	118%	17%	0%	10%	0%	67%	0%	2%	0%	29%	18%
5 h ahead	19%	26%	0%	0%	102%	107%	58%	0%	36%	0%	84%	21%	8%	0%	44%	22%
6 h ahead	48%	78%	0%	0%	97%	86%	65%	45%	51%	0%	122%	64%	10%	16%	56%	41%
	19%		25%		67%		0%		0%		81%		8%			
2 d (next day)	25%	25%	40%	22%	103%	88%	34%	10%	31%	15%	85%	95%	3%	5%	46%	37%
3 d	37%	26%	42%	21%	113%	84%	35%	10%	41%	15%	114%	97%	26%	8%	58%	37%
4 d	24%	26%	49%	21%	129%	83%	39%	10%	43%	10%	128%	102%	20%	10%	62%	38%
5 d	18%	26%	59%	21%	135%	83%	64%	5%	67%	10%	139%	102%	25%	10%	72%	37%
6 d	29%	25%	75%	21%	151%	90%	109%	15%	85%	5%	128%	102%	43%	11%	89%	38%
7 d	38%	25%	82%	21%	153%	95%	124%	14%	106%	0%	124%	103%	60%	10%	98%	38%

The breakeven point between cloud-motion and NDFD forecasts is 5– 6 h ahead, consistent with previous observations by Lorenz et al. (2007). We note, however, that satellite-aided multiple output statistics (MOS), real-time feedback, and assimilation procedures (e.g., Dennstaedt 2006), whereby the NWP forecasts are corrected from the most recent satellite-derived irradiance history, could improve the NDFD forecasts. Such an assimilation process has not yet been implemented in the SolarAnywhere forecasts.

The cloud-motion forecasts' MBE is consistently small, with the exception of sites experiencing important winter snow cover, where the accuracy of the current satellite model, which relies solely on the visible channel, is limited. A new model developed by the authors that utilizes both infrared and visible channels will eliminate such bias (Perez et al. 2010a). However,this new version of the model (SolarAnywhere V.3) was not operational at the time of the evaluation.

The NDFD bias exhibits a seasonal pattern as well as site dependence: The bias is smallest for the sites that experience either little cloud cover or a fast-passing frontal-type cloud cover such as that experienced in the Western United States and the Great Plains. The eastern sites, such as Penn State and Goodwin Creek, where localized cloud formation occurs more frequently, exhibit a tendency to negative bias. The seasonal pattern shows that the NDFD forecasts have a tendency toward positive irradiance bias in the fall (cloudiness underprediction) and negative bias in the other seasons, particularly in the spring (cloudiness overprediction). Despite these shortcomings, the NDFD forecasts perform considerably better than persistence up to 6 d ahead.

The KSI and OVER metrics are important for site characterization because they define the ability of a model to adequately re-create the observed distribution of clear, partly cloudy, and overcast events. Such information is important for design purposes, but is less important for forecast operations where the short-term accuracy metrics (RMSE and MAE) are the key performance factors in quantifying the ability of a model to forecast changes ahead. The use of distribution metrics within a forecasting context simply serves as a check to ensure that the models have a reasonable physical foundation.

The 1 h persistence-forecast time series is simply the measured time series itself moved 1 h forward and modified only by solar-geometry effects. As a result, it is neither surprising nor concerning that the persistence-based forecasts tend to score better than both the cloud-motion and NDFD forecast models when evaluated using the KSI and OVER metrics. Indeed, for very short term same-day forecasts, the statistical distribution of persistence forecasts should be almost identical to measurements. One notable exception is Boulder, where the very marked diurnal patterns produce different statistical distributions for different times of day and where cloud motion

provides better results. The 1–6 d-ahead persistence forecast also exhibits a better performance than the NDFD when assessed via the KSI and OVER metrics. As for cloud motion, the NDFD distribution statistics deteriorate sensibly with the time horizon, reflecting a loss of dynamic range for the latter[8] and the possible existence of systematic daily patterns for the former. This is due to pixel convergence/averaging in the case of cloud motion and likely due to the natural tendency of models and forecasters to avoid extreme forecasts (clear or cloudy) as the time horizon increases for the NDFD models.

10.3.2. Extended-Area Validations

The extended-area validation is largely qualitative and focuses on the ability of the forecast models to account for the solar resource's microclimatic features over a given period. The validation criterion is a visual evaluation of the mapped solar resource computed from ongoing forecast data. Because we do not have gridded instrumentation spanning the considered areas, we rely on satellite-derived irradiance data as a performance benchmark.

We consider $2^o \times 2^o$ regions ($\sim$15,000 km^2) surrounding two ground-truth stations, Boulder and Desert Rock, which have the strongest microclimatic features that are driven by orography or terrain. Figure 10.6 compares the mapped irradiances for Desert Rock in summer and for Boulder in the fall, spring, and year-round. The maps consist of the satellite model, the 1 and 3 h cloud-motion forecasts, and forecasts for next day, three days, and six days ahead. The orographic features that may influence the solar resource—with cloud buildup expected to prevail around the most important ridges—are shown in Figure 10.7.

The NDFD model does account for orography-driven microclimates but apparently only when cloudiness increases with elevation. This underlying assumption is appropriate in Desert Rock in summer and in spring in Boulder. However, in the fall of 2008, clouds preferentially formed immediately east of the Rocky Mountains, likely linked to the presence of easterly winds leading to "upslope" cloud formation. This preferential cloud-formation trend is not taken into account by the NDFD models.The smoothing effect of cloud motion tends to erase some of the terrain features (pixel convergence and averaging).

Finally, Figure 10.6 also shows the discontinuities inherent to the NDFD process, whereby global forecasts are modified independently by regional offices before being reassembled on the NDFD grid. The discontinuity at a small portion of the top of the Boulder maps (appearing as a horizontal

8. The loss of dynamic range reflects the tendency of the NDFD forecasters to increasingly "hedge" their forecasts as the time horizon increases.

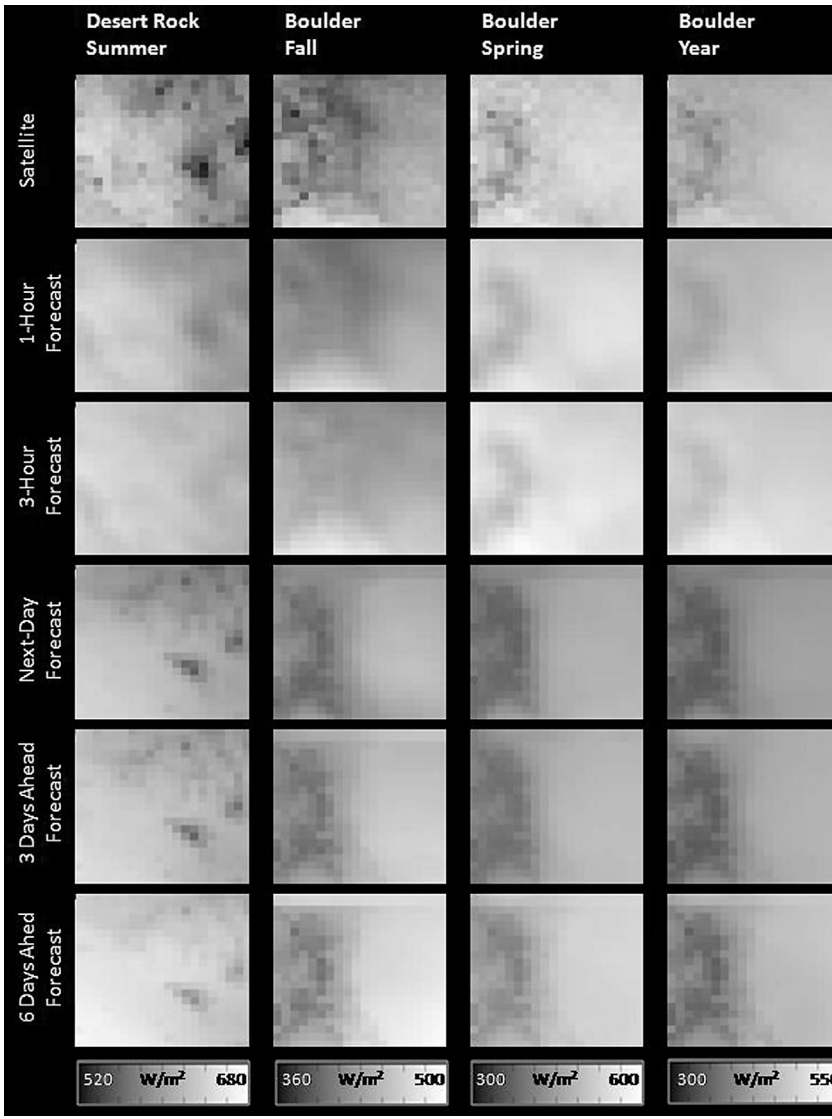

FIGURE 10.6 Long-term-average GHI from in a $2^{o} \times 2^{o}$ region surrounding the Boulder and Desert Rock sites for the satellite model, cloud-motion forecasts (1, 3 h ahead), and NDFD (1, 3, 6 d ahead).

discontinuity for time horizons greater than or equal to the next-day forecast) marks the boundary between two U.S. National Weather Service offices producing a different assessment of local cloudiness that becomes apparent over integrated timescales.

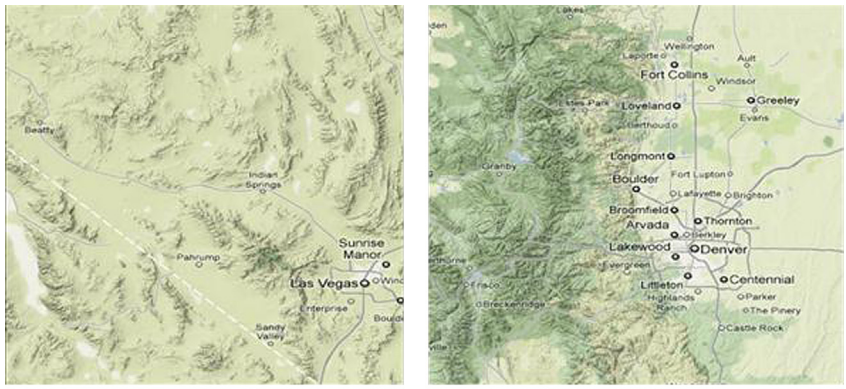

FIGURE 10.7 Orographic features in the regions analyzed in Figure 10.6. *This figure is reproduced in color in the color section.*

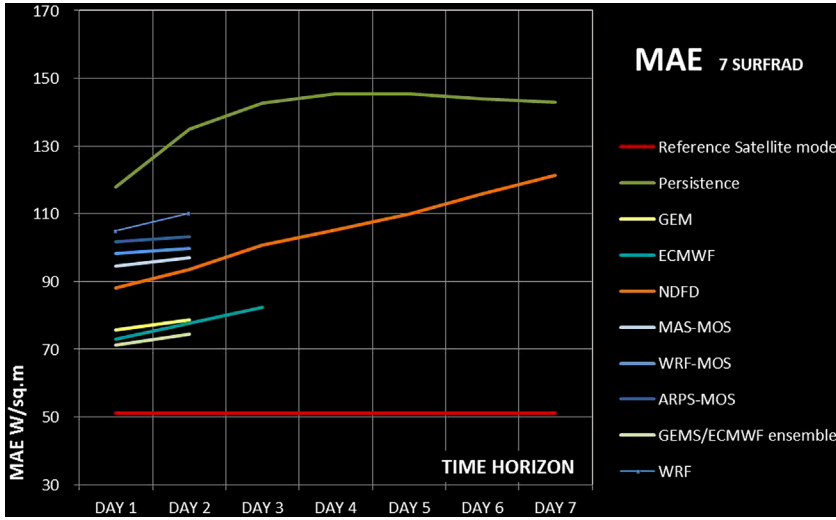

FIGURE 10.8 Contrasting the performance of SolarAnywhere's NDFD-based forecast with the performance of GFS-driven mesoscale models (WRF, MASS, and ARPS) as well as European and Canadian global models (ECMWF and GEM) using MAE as a metric. *This figure is reproduced in color in the color section.*

10.3.3. Intercomparison of NWP Solar Forecast Models

An operational performance context for SolarAnywhere's NDFD forecasts was recently provided by the authors and a team of researchers from the International Energy Agency's Solar heating and Cooling Programme's Task 36 (IEA-SHCP 2010, Perez et al. 2011, Lorenz et al. 2009, Pelland et al. 2011). In this context, multiday GHI NWP forecast models were intercompared in the

TABLE 10.5 Comparison of Multiday GHI NWP Forecast Models

	Forecast models	Time horizon
EUROPE		
Germany	ECMWF[a]	3 days
	WRF-Meteotest[b]	3 days
	BLUE FORECAST[c]	3 days
	CENER[d]	2 days
Switzerland	ECMWF[a]	3 days
	WRF-Meteotest[b]	3 days
	BLUE FORECAST[c]	3 days
Austria	ECMWF[a]	3 days
	WRF-Meteotest[b]	3 days
	BLUE FORECAST[c]	3 days
	CENER[d]	2 days
	Meteorologists[e]	2 days
Spain	ECMWF[a]	3 days
	WRF-UJAEN[b]	3 days
	BLUE FORECAST[c]	3 days
	CENER[d]	2 days
	HIRLAM[f]	3 days
USA	GEM[g]	2 days
	ECMWF[a]	3 days
	WRF and WRF-ASRC	2 days
	MASS[h]	2 days
	ARPS[i]	2 days
	NDFD[j]	7 days
CANADA	GEM[g]	2 days
	ECMWF[a]	2 days
	WRF-ASRC[b]	2 days

[a] *An application of the ECMWF model (ECMWF 2010).*
[b] *Several versions of the WRF model (WRF 2010) initialized with GFS (GFS 2003) forecasts from NCEP.*

- A version used as part of an operational air-quality forecasting program at the University of Albany (WRF-ASRC) (Skamarock et al. 2005, Air Quality Forecast Modeling System 2010).
- A version operated at AWS TruePower in the United States (WRF).
- A version operated at Meteotest in Europe (WRF-Meteotest).
- A version operated at the University of Jaén (WRF-UJAEN).

[c] *A statistical forecast tool of Bluesky based on the GFS (GFS 2003) model of the NCEP (Natschläger et al. 2008).*
[d] *Forecasts of CENER derived with a statistical postprocess based on learning machines applied to the regional weather forecasting system Skiron.(Kallos 1997).*
[e] *Forecasts based on meteorologists' cloud-cover forecasts by Bluesky, Austria.*

TABLE 10.5 Comparison of Multiday GHI NWP Forecast Models—cont'd

Forecast models	Time horizon

[f]*The High-Resolution Limited Area Model (HIRLAM 2012) operational model from the Spanish Weather Service (AEMet) combined with a statistical postprocessing at Ciemat, Spain.*
[g]*The Global Environmental Multiscale (GEM) model from Environment Canada in its regional deterministic configuration (Mailhot et al. 2006).*
[h]*A proprietary mesoscale model, the MASS model (MESO 2010).*
[i]*The Advanced Multiscale Regional Prediction System (ARPS) model (Xue et al. 2001).*
[j]*A model based on cloud cover predictions from the NDFD (NDFD 2010).*

United States, Canada, and Europe. These models are listed in Table 10.5; two of them—the ECMWF global model (ECMWF 2010) and the GFS-driven WRF mesoscale model (WRF 2010)—were common to the three regional intercomparisons in Canada, the United States, and Europe, thus providing a common reference that could be used to draw the following general observations:

- The performance of mesoscale models driven by NOAA's GFS global model tends to lag the performance of models driven by other global models, namely ECMWF and GEM. The latter exhibit a systematic MAE (RMSE) reduction of 5%–10% (10%–15%) when compared to GFS-driven models.[9]
- The higher-resolution mesoscale models such as WRF do not appear, at this stage of their development, to improve day-ahead and multiday-ahead performance when compared to lower-resolution global models.
- All models score considerably better than persistence, with a systematic MAE (RMSE) reduction of 20%–25% (35%–40%) for the best global models on same-day forecasts and larger gains on multiday forecasts.
- An elementary ensembling of the best-performing models (e.g., ECMWF and GEM) leads to an additional MAE (RMSE) reduction of 2%–4% (5%–8%).

A model comparison summary for North America is shown in Figure 10.5.

9. Note that the IEA team did not compare the GFS global model directly to the other global models, but only its application via mesoscale models or the NDFD. Mathiesen and Kleissl (2011) have shown that the standalone GFS model should indeed perform better than through-the-filter mesoscale models, which tend to introduce unwarranted dispersion error at this stage of their irradiance-modeling development.

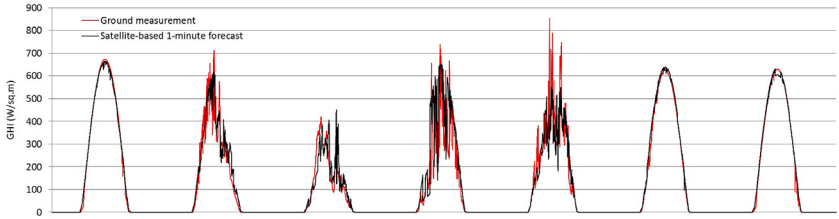

FIGURE 10.9 Measured and satellite-derived forecast for the test week over a 7-d time period with a time horizon of 1–30 min. *This figure is reproduced in color in the color section.*

10.4. PERFORMANCE EVALUATION: 1 KM, 1 MIN FORECASTS

We present a preliminary evaluation of SolarAnywhere High Resolution (SA Hi Res), a new product undertaken as part of a California Energy Commission project on utility-scale renewable energy integration (CEC 2012). The SolarAnywhere High-Resolution tool produces high-frequency (1 min) irradiance forecasts at 1 km ground resolution up to 1 h ahead.

Unlike hourly or half-hourly forecasts, the ability to predict the minute-specific power-output time series is not the most important forecast-validation criterion. The strength of the forecast at this high-frequency level resides in accurately predicting the variability of the resource relative to some predicted mean value. The standard measure of dispersion between measured and predicted time series (RMSE or MAE) is pertinent in evaluating

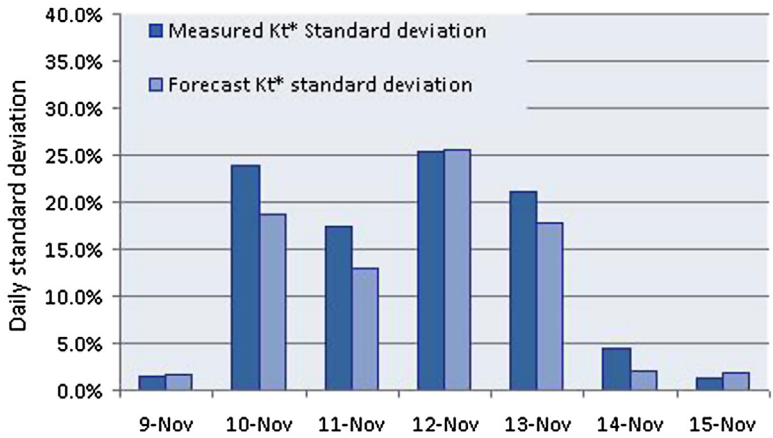

FIGURE 10.10 Comparing measured σKt^* (*top*) and $\sigma \Delta Kt^*$ (*bottom*) predictions of 1 min data for each day in the test week. The considered time period Δt is 1 min; the time period over which the standard deviations are computed is 1 d; and the considered forecast time horizon is 0–30 min. *This figure is reproduced in color in the color section.*

minute-specific prediction performance. However, to assess the performance of short-term variability prediction, it is more important to compare the predicted and actual standard deviations of the clear-sky index (σKt^*) and the standard deviations of changes in it ($\sigma \Delta Kt^*$). Hoff (2011) shows that capturing both parameters is sufficient to quantify the grid impact of arbitrary PV fleets from a single system to an extended distribution of arrays.

Figure 10.9 is a qualitative evaluation of the SA Hi Res forecasts for one test week at a location in the southwestern United States, comparing up to 1/2 h-ahead forecasts to ground measurements. The figure presents the measured-irradiance data and the satellite-based 1 min resolution forecasts refreshed every 1/2 hour when a new satellite image is available.

Figure 10.10 is a quantitative evaluation of the model, illustrating its capability to predict the solar-resource variability metrics (σKt^* and $\sigma \Delta Kt^*$) with a half-hour time horizon. Results show that the model adequately forecasts these key operational parameters that are used as input to PV-fleet probabilistic-forecast models (Hoff 2012).

CONCLUDING REMARKS

This chapter described, and presented a validation of, the SA forecast chain of models in its current (2012–2013) operational configuration. The individual forecast models will likely evolve as the state of the art pushes forward. However, the main originality of the SA forecast platform—to provide a seamless continent-wide platform to serve historical, real, short-term and longer-term forecasts, and to interface this platform with the monitoring and forecasting of an entire fleet of solar systems—will remain.

REFERENCES

Air Quality Forecast Modeling System, 2010. http://asrc.albany.edu/research/aqf/.

California Energy Commission(CEC), 2012. Demonstration and Validation of PV Output Variability Modeling Approach. Project # 500-10-059.

Clean Power Research, 2012. SolarAnywhere. www.solaranywhere.com.

Dennstaedt, S., 2006. Model Output Statistics Provide Essential Data for Small Airports. The Front 6 (2), 1–4.

Espinar, B., Ramírez, L., Drews, A., Beyer, H.G., Zarzalejo, L.F., Polo, J., Martín, L., 2008. Analysis of different error parameters applied to solar radiation data from satellite and German radiometric stations. Solar Energy vol. 83 (Issue 1), 2009.

European Centre for Medium-Range Weather Forecasts (ECMWF), 2010. http://www.ecmwf.int/.

Global Forecast System (GFS), 2003. Environmental Modeling Center. NOAA, Washington, DC. http://www.emc.ncep.noaa.gov/gmb/moorthi/gam.html.

HIRLAM, 2012. High Resolution Limited Area Model. http://hirlam.org.

Hoff, T.E., 2011. Computer-Implemented System and Method for Determining Point-to-Point Correlation of Sky Clearness for Photovoltaic Power Generation Fleet Output Estimation (Patent No. US 8,165,811 B2), Computer-Implemented System and Method for Estimating

Power Data for a Photovoltaic Power Generation Fleet (Patent No. US 8,165,812 B2). Computer-Implemented System and Method for Efficiently Performing Area-to-Point Conversion of Satellite Imagery for Photovoltaic Power Generation Fleet Output Estimation (Patent No. US 8,165,813 B2). U.S. Patents.

Hoff, T.E., Perez, R., Kleissl, J., Renne, D., Stein, J., 2012. Reporting of irradiance modeling relative prediction errors. Prog. Photovolt: Res. Appl. Wiley Online Library. wileyonlinelibrary.com.

Hoff, T.E., Perez, R., 2013. Evaluating Satellite-Derived and Measured Irradiance Accuracy for PV Resource Management in the California Independent System Operator Control Area. Progress in Photovoltaics (pending final review).

IEA-SHCP, 2010. Task 36 Final Report, Subtask A - Standard Qualification for Solar Resource Products.

Kallos, G., October 1997. The Regional weather forecasting system SKIRON. Proceedings, Symposium on Regional Weather Prediction on Parallel Computer Environments, 15–17. Athens.

Kasten, F., Czeplak, G., 1979. Solar and Terrestrial Radiation dependent on the Amount and type of Cloud. Solar Energy 24, 177–189.

Lorenz, E., Heinemann, D., Wickramarathne, H., Beyer, H.G., Bofinger, S., 2007. Forecast of Ensemble Power production by Grid-connected PV Systems. Proc. 20th European PV Conference, Milano, Italy.

Lorenz, E., Remund, J., Müller, S.C., Traunmüller, W., Steinmaurer, G., Pozo, D., Ruiz-Arias, J.A., Lara Fanego, V., Ramirez, L., Romeo, M.G., Kurz, C., Pomares, L.M., Guerrero, C.G., 2009. Benchmarking of Different Approaches to Forecast Solar Irradiance, Proceedings of the 24th European Photovoltaic Solar Energy Conference, 21–25. September 2009, Hamburg.

Mailhot, J., Bélair, S., Lefaivre, L., Bilodeau, B., Desgagné, M., Girard, C., Glazer, A., Leduc, A.M., Méthot, A., Patoine, A., Plante, A., Rahill, A., Robinson, T., Talbot, D., Tremblay, A., Vaillancourt, P.A., Zadra, A., 2006. The 15-km version of the Canadian regional forecast system. Atmosphere-Ocean 44, 133–149.

Mathiesen, P., Kleissl, J., 2011. Evaluation of numerical weather prediction for intra-day solar forecasting in the continental United States. Solar Energy 85, 967–977.

Meso, 2010. Mesoscale Amospheric Simulation System – MASS. www.meso.com.

National Institute of Standards and Technology (NIST), 2010. Engineering and Statistics Handbook. www.itl.nist.gov.

National Weather Service, NOAA, 2010. The SURFRAD Network Monitoring Surface Radiation in the Continental United States. Washington, DC.

National Weather Service, NOAA, 2010. National Forecast Database (NDFD) Washington, DC. http://www.weather.gov/ndfd/.

Natschläger, T., Traunmüller, W., Reingruber, K., Exner, H., 2008. Lokal optimierte Wetterprognosen zur Regelung stark umweltbeeinflusster Systeme; SCCH, Blue Sky. Tagungsband Industrielles Symposium Mechatronik Automatisierung, 281–284. Clusterland Oberösterreich GmbH / Mechatronik-Cluster. 2008.

Pelland, S., Gallanis, G., Kallos, G., 2011. Solar and Photovoltaic Forecasting through Post-Processing of the Global Environmental Multiscale Numerical Weather Prediction Model. Submitted to Progress in Photovoltaics. Research and Applications.

Perez, R., Ineichen, P., Moore, K., Kmiecik, M., Chain, C., George, R., Vignola, F., 2002. A New Operational Satellite-to-Irradiance Model. Solar Energy 73 (5), 307–317.

Perez, R., Ineichen, P., Kmiecik, M., Moore, K., George, R., Renne, D., 2004. Producing satellite-derived irradiances in complex arid terrain. Solar Energy 77 (4), 363–370.

Perez, R., Kivalov, S., Zelenka, A., Schlemmer, J., Hemker Jr., K., 2010. Improving the Performance of Satellite-to-Irradiance Models Using the Satellite's Infrared Sensors. Proc. of American Solar Energy Society's Annual Conference, Phoenix, AZ.

Perez, R., Kivalov, S., Schlemmer, J., Hemker Jr., K., Renne, D., Hoff, T., 2010b. Validation of Short and Medium Term Operational Solar Radiation Forecasts in the US. Solar Energy 84 (12), 2161–2172.

Perez, R., Moore, K., Wilcox, S., Renné, D., Zelenka, A., 2007. Forecasting Solar Radiation – Preliminary Evaluation of an Approach Based upon the national Forecast Data Base. Solar Energy 81 (6), 809–812.

Perez, R., Beauharnois, M., Hemker Jr., K., Kivalov, S., Lorenz, E., Pelland, S., Schlemmer, J., Van Knowe, G., 2011. Evaluation of Numerical Weather Prediction Solar Irradiance Forecasts in the US. Proc. Solar 2011, American Solar Energy Society's Annual Conference.

Skamarock, W.C., Klemp, J.B., Dudhia, J., Gill, D.O., Barker, D.M., Wang, W., Powers, J.G., 2005. A Description of the Advanced Research WRF Version 2, NCAR Technical Note: NCAR/TN–468+STR. National Center for Atmospheric Research, Boulder, Colorado.

Stuhlmann, R., Rieland, M., Raschke, E., 1990. An improvement of the IGMK model to derive total and diffuse solar radiation at the surface from satellite data. Journal of Applied Meteorology 29, 586–603.

WRF, 2010. Weather research and forecasting (WRF) model. http://www.wrf-model.org.

Xu, K.M., Randall, D.A., 1996. A semiempirical cloudiness parameterization for use in climate models. J. Atmos. Sci. 53, 3084–3102.

Xue, M., Droegemeier, K.K., Wong, V., Shapiro, A., Brewster, K., Carr, F., Weber, D., Y.Liu, Wang, D.-H., 2001. The Advanced Regional Prediction System (ARPS) - A multiscale nonhydrostatic atmospheric simulation and prediction tool. Part II: Model physics and applications. Meteorology and Atmospheric Physics 76, 134–165.